https://doi.org/10.5194/egusphere-2026-5325
Preprint. Discussion started: 9 September 2026

Theory for Optically Observing Cloud Aerosol Critical Activation Diameter

Ye Kuang[1], Qi Liu[1]

[1] Institute for Environmental and Climate Research, College of Environment and Climate, Jinan University, Guangzhou, 511443, Guangdong, China.

Correspondence: Ye Kuang (kuangye@jnu.edu.cn)

Abstract:

Aerosol activation is the fundamental microphysical process governing cloud droplet formation. The critical activation diameter, D_a, is a key parameter that characterizes cloud supersaturation and aerosol activation and serves as a fundamental variable in simulations of aerosol–cloud interactions. Kuang et al. (2025) proposed a machine-learning framework for the instantaneous retrieval of D_a from spectral scattering measurements of interstitial and activated aerosols. However, the lack of a rigorous theoretical foundation has limited the understanding of the method's physical basis, applicability, and limitations in field observations. Here, we establish the missing theoretical foundation by integrating aerosol activation theory with Mie scattering theory to derive a unified closed-form solution linking optical scattering to the D_a. The resulting theory provides the first analytical explanation for the approximately linear relationship between D_a and the scattering fraction of interstitial aerosols reported by Kuang et al. (2025), while also revealing the strongly nonlinear behavior near the limiting scattering regimes. Furthermore, the theoretical detection limit of the optical approach is quantified, and its potential applicability to different cloud types is evaluated. Overall, this work provides a rigorous theoretical foundation for optical observations of cloud aerosol activation. The unified analytical solution bridges all limiting regimes, clarifies the physical basis of optical retrievals of the critical activation diameter, and offers theoretical guidance for the design and optimization of future optical instruments for cloud activation measurements.

https://doi.org/10.5194/egusphere-2026-5325
Preprint. Discussion started: 9 September 2026

1. Introduction

Aerosol-cloud interactions are fundamental for cloud physics and play significant roles in weather modifications (Kreidenweis et al., 2018) and climate change projections (Fan et al., 2016). Aerosol activation plays a critical role in aerosol-cloud interactions which determines the number of cloud droplets and thus constitutes the central concept of the classical Twomey theory (Twomey, 1959). The critical activation diameter (D_a) is the most important parameter in quantifying cloud droplet number concentrations with given aerosol particle number size distributions in models (Abdul-Razzak et al., 1998;Abdul-Razzak and Ghan, 2000, 2002) and also the key parameter in constraining aerosol activation properties and estimating effective supersaturation in clouds (Ditas et al., 2012;Hammer et al., 2014;Zíková et al., 2020;Wainwright et al., 2021;Dedrick et al., 2025).

Theoretically, on the basis of Köhler activation theory, D_a is mostly determined by aerosol hygroscopicity and the supersaturation experienced by aerosols. In clouds, supersaturation might fluctuate quickly, which result in quick changes of aerosol activation processes, therefore high-time-resolution observations are necessary for D_a observations. Several methods have been proposed to observe D_a in clouds/fogs. The direct way is to observe size-resolved activation ratio using aerosol size distribution techniques in combination with different sampling inlets and adryer system. For example, the combination of total suspended particle (TSP) inlet with the cloud droplet sampling, such as Ground-based Counterflow Virtual Impactor (GCVI) (Noone et al., 1988) and Pumped Counterflow Virtual Impactor (PCVI) (Boulter et al., 2006;Motos et al., 2019a). Another way could also achieve this purpose by integrating TSP and normal impactors which allow interstitial aerosols to be sampled (Henning et al., 2004;Motos et al., 2019b;Zíková et al., 2020), for example, the impactors with aerodynamic cutoff diameter of 1 μm and 2.5 μm (PM_1 and $PM_{2.5}$). Despite the differences of sampling inlets, it is not the fundamental reason that affects the high time resolution and even vertical observations of D_a because multiple inlets could be used simultaneously to overcome the inlet limitations. The key issue is that the accurate aerosol size distribution usually needs minutes level to finish the scanning procedure, for example, the most popular scanning mobility particle sizer (SMPS). Other optical techniques could achieve the seconds level observations of aerosol size distributions; however, their size ranges are generally limited. For example, the aerodynamic particle sizer (APS) could only cover size range of larger than about 500 nm, and some other low-cost optical particle counter which are rarely capable of extending the size range down to 100 nm (Gao et al., 2013). In addition, these optical techniques usually bear uncertainties of diameter conversion which could be significantly impacted by aerosol properties such as refractive index and density.

https://doi.org/10.5194/egusphere-2026-5325
Preprint. Discussion started: 9 September 2026

Other methods were also used to indirectly infer D_a and could not achieve online estimations. For example, using the observed cloud number concentrations and aerosol size distributions to estimate D_a. This approach integrates the out-of-cloud or below-cloud aerosol PNSD from the largest diameter downward until the integral matches the measured in-cloud droplet number concentration (Mazoyer et al., 2019;Dedrick et al., 2025). However, this method suffers from biases caused by spatial and temporal variabilities of aerosols in clouds and neglecting the non-linear activated-curve transition caused by chemical heterogeneity of aerosol population. In addition, the Hoppel Minimum Method was also used to estimate D_a. It estimates D_a experimentally from aerosol size distribution measurements by identifying the Hoppel minimum, a morphological valley separating the Aitken and accumulation modes (Gong et al., 2023). While the applicability of this method in different regions and seasons needs further verification. Especially, this distinctive bimodal structure might be frequently obscured by primary emissions and secondary particle formation in complex continental environments (Cai et al., 2020;Hou et al., 2026).

In summary, a new theory and method is urgently needed to achieve the high-time-resolution D_a observations in clouds. The optical machine learning method proposed in Kuang et al. (2025) matches this requirement. The physical thinking of this method has been made clear in Kuang et al. (2025), however, the detailed theoretical foundations of this method need further clarifications and its potential applications and limitations in field cloud measurements need to be further explored in a theoretical way to guide the future optical instrument design. This study addresses this aspect by clearly deducing the relationships between scattering properties of inactivated and activated aerosols and D_a directly from the combination of the Mie theory and activation theory. The theoretical analysis explains clearly the physical connections between D_a and the dry-state scattering fractions of interstitial aerosols in total aerosol populations and could pave the way for sophisticated optical instrument development that aims for aerosol activation observations in clouds.

2. Theoretical formulations

2.1 Analytical Formulation of the Interstitial aerosol Scattering Fraction

The results of Kuang et al. (2025) demonstrated clear observational evidence that the D_a is almost linearly correlated with the submicron scattering fraction of interstitial aerosols (f_{sp}) in the total aerosol populations which depends on the scattering Ångström exponent (SAE) which are determined mainly by the shape of aerosol size distribution. The qualitative physical intuition behind this phenomenon is that the larger the D_a, the higher the f_{sp} and their relationships are likely shaped by aerosol size distributions (Kuang et al., 2018) which could be constrained by spectral scattering measurements of

https://doi.org/10.5194/egusphere-2026-5325
Preprint. Discussion started: 9 September 2026

aerosols. However, the theoretical understanding behind these linear relationships as well as the application boundaries of this optical method need to be further clarified. Here, we address this by establishing a theoretical framework that starts from connecting f_{sp} and D_a on the basis of Mie theory and aerosol activation theory.

The f_{sp} is formally defined as the scattering ratio of interstitial aerosols to the total scattering of submicron aerosols:

$$f_{sp} = \frac{\int_{-\infty}^{\infty}[1 - F_{act}(D_p)]\frac{d\sigma_{sp}(\lambda)}{d\ln D_p}d\ln D_p}{\int_{-\infty}^{\infty}\frac{d\sigma_{sp}(\lambda)}{d\ln D_p}d\ln D_p} \quad (1)$$

where $F_{act}(D_p)$ represents size-resolved aerosol activation ratios and $\sigma_{sp}(\lambda)$ represents the aerosol scattering coefficient at wavelength λ, $F_{act}(D_p)$ could be represented using the error function:

$$F_{act}(D_p) = \frac{\mathrm{MAF}}{2}\left[1 + \mathrm{erf}\left(\frac{\ln D_p - \ln D_a}{\sqrt{2}\ln\sigma_a}\right)\right] \quad (2)$$

where MAF is the maximum activation fraction and $\ln\sigma_a$ represents activation broadening associated with chemical composition heterogeneity (Tao et al., 2018), turbulence (Shawon et al., 2021;Anderson et al., 2023) and even supersaturation history that droplets have been experienced (Kuang et al., 2025). Note that this form is slightly different with the typical error function that were usually used in fitting size-resolved activation ratio measurements (Rose et al., 2008) which is discussed in Sect.S1 and the slight change is for the purpose of explicitly integrating.

While the explicit formula of $F_{act}(D_p)$ is convenient, the challenge remains for size-resolved aerosol scattering due to the nonlinear responses of aerosol scattering to size changes. It was well known that aerosol scattering is generally proportional to volume for submicron aerosols (Kuang et al., 2018) and size-resolved aerosol scattering is mainly shaped by the aerosol volume size distribution (Kuang et al., 2020) which is in general dominantly contributed by accumulation mode aerosols (Bian et al., 2014) for submicron aerosols. These characteristics resulted in that submicron aerosol volume size distributions could be generally represented using a lognormal distribution. Therefore, we first express the volume size distribution $v(D_p)$ as:

$$v(D_p) = \frac{V_{tot}}{\sqrt{2\pi}\ln\sigma_g}\exp\left(-\frac{(\ln D_p - \ln D_{g,v})^2}{2\ln^2\sigma_g}\right) \quad (3)$$

https://doi.org/10.5194/egusphere-2026-5325
Preprint. Discussion started: 9 September 2026

where V_{tot} is the total aerosol volume concentration, $D_{g,v}$ is the volume geometric mean diameter, and σ_g is the geometric standard deviation. According to the Mie theory, the scattering efficiency parameter Q_{sca} for a dielectric sphere is an infinite multipole expansion:

$$Q_{sca}(x,m) = \frac{2}{x^2}\sum_{n=1}^{\infty}(2n+1)\left(|a_n(x,m)|^2 + |b_n(x,m)|^2\right) \quad (4)$$

where $x = \pi D_p/\lambda$ is the dimensionless size parameter, m is the complex refractive index, and a_n and b_n are the Mie scattering coefficients. At visible wavelengths, accumulation mode aerosols that contribute most (Kuang et al., 2018) to submicron aerosol scattering (100-800 nm) fall within the primary Mie resonance transition zone ($x \sim 1$). Applying a first-order logarithmic Taylor expansion near the accumulation mode centroid simplifies results of Equation (4) to a generalized power-law approximation:

$$Q_{sca}(D_p) \approx C(m,\lambda)\cdot D_p^{k_{mie}} \quad (5)$$

where $k_{mie} = \partial \ln Q_{sca}/\partial \ln D_p$ is the local scaling exponent and sometimes approximated as 1 for simplification (Kuang et al., 2020). The parameter C stems analytically from the multipole expansion and accounts for roles of wavelength and refractive index. Given these analytical formulations, the scattering cross-section of a single particle $C_{sca}(D_p)$ relates to its volume ($V = \frac{\pi}{6}D_p^3$) via $C_{sca}(D_p) = Q_{sca}(D_p)\cdot\pi\cdot(D_p/2)^2 = Q_{sca}(D_p)\cdot\frac{3}{2D_p}\cdot V$. Therefore, size-resolved aerosol scattering could be expressed as:

$$\frac{d\sigma_{sp}}{d\ln D_p} = \frac{3}{2D_p}Q_{sca}(D_p)v(D_p) = \frac{3C}{2}D_p^{k_{mie}-1}v(D_p) \quad (6)$$

Substitute Eq.4 and 6 into Eq.1, an integral equation that relates f_{sp} to D_a yields. Multiplying a log-normal distribution by D_p^n ($n = k_{mie} - 1$) yields an identically shaped, shifted distribution with its geometric mean scaled by $\exp(n\ln^2\sigma_g)$. Setting the new optical peak diameter as the scattering equivalent mean diameter ($D_{g,sca}$), which could be explicitly formulated as:

$$D_{g,sca} = D_{g,v}\exp\left((k_{mie}-1)\ln^2\sigma_g\right) \quad (8)$$

when $k_{mie} = 1$, the scattering peak diameter aligns perfectly with the volume peak diameter ($D_{g,sca} = D_{g,v}$).

https://doi.org/10.5194/egusphere-2026-5325
Preprint. Discussion started: 9 September 2026

To solve this integral, we normalize the scattering kernel by defining the Optical Scattering Size Distribution (OSSD), $p_{sca}(\ln D_p)$, as a probability density function:

$$p_{sca}(\ln D_p) = \frac{\frac{d\sigma_{sp}(\lambda)}{d\ln D_p}}{\int_{-\infty}^{\infty} \frac{d\sigma_{sp}(\lambda)}{d\ln D_p} d\ln D_p} \tag{9}$$

Since $p_{sca}(\ln D_p)$ would be integrated as 1 over the whole space and forms a log-normal distribution centered at $\ln D_{g,sca}$ with a standard deviation of $\ln\sigma_g$, the f_{sp} formula simplifies to:

$$f_{sp} = 1 - \int_{-\infty}^{\infty} F_{act}(D_p) p_{sca}(\ln D_p) d\ln D_p \tag{10}$$

Substituting the activation function $F_{act}(D_p)$ into Equation (10) yields:

$$f_{sp} = 1 - \frac{\mathrm{MAF}}{2} - \frac{\mathrm{MAF}}{2} \int_{-\infty}^{\infty} \mathrm{erf}\left(\frac{\ln D_p - \ln D_a}{\sqrt{2}\ln\sigma_a}\right) p_{sca}(\ln D_p) d\ln D_p \tag{11}$$

To solve this integral analytically, we utilize the mathematical convolution identity for Gaussian and error functions:

$$\int_{-\infty}^{\infty} \mathrm{erf}(Ax + B) \frac{1}{\sqrt{2\pi}\sigma_s} e^{-\frac{(x-\mu_s)^2}{2\sigma_s^2}} dx = \mathrm{erf}\left(\frac{A\mu_s + B}{\sqrt{1 + 2A^2\sigma_s^2}}\right) \tag{12}$$

By mapping the physical variables to the mathematical identity using $x = \ln D_p$, the log-normal OSSD p_{sca} translates to a normal distribution with mean $\mu_s = \ln D_{g,sca}$ and variance $\sigma_s^2 = \ln^2\sigma_g$. The arguments of the error function map to $A = 1/(\sqrt{2}\ln\sigma_a)$ and $B = -\ln D_a/(\sqrt{2}\ln\sigma_a)$. We define the orthogonal sum of the size distribution width and the activation width as the total broadening factor σ_d:

$$\sigma_d = \sqrt{\ln^2\sigma_g + \ln^2\sigma_a} \tag{13}$$

Utilizing the property $\mathrm{erf}(-x) = -\mathrm{erf}(x)$ to handle the logarithmic terms, the exact closed-form expression for f_{sp} could be finally derived as:

$$f_{sp} = 1 - \frac{\mathrm{MAF}}{2} + \frac{\mathrm{MAF}}{2} \mathrm{erf}\left(\frac{\ln D_a - \ln D_{g,sca}}{\sqrt{2}\sigma_d}\right) \tag{14}$$

Which explicitly relates f_{sp} to D_a. As discussed before both $D_{g,sca}$ and σ_g are essential volume size distribution parameters.

https://doi.org/10.5194/egusphere-2026-5325
Preprint. Discussion started: 9 September 2026

2.2 Linking Scattering Spectral dependence to Aerosol volume Size Distributions

While Equation (14) establishes a physical linkage, an optical retrieval requires parameterizing $D_{g,v}$ with optical measurables. It was well known that a strong relationship exists between the aerosol mean size and the scattering spectral dependence of aerosols, and this dependence was usually characterized by SAE as aforementioned. If scattering spectra cover wide ranges of wavelengths or angles could be measured, aerosol size distribution could even be directly retrieved through Mie scattering closure (Espinosa et al., 2017). However, aerosol scattering of limited wavelengths was usually measured and made only constant SAE available. For example, multiple wavelength nephelometer was usually applied for this purpose. Given this, we define a proxy function χ that expresses $D_{g,v}$ using SAE and the σ_g:

$$\log_{10}(D_{g,v}) = \chi(\mathrm{SAE}, \sigma_g) \tag{15}$$

This definition helps transform the size parameter into an optically derivable quantity. Substituting this proxy for $D_{g,v}$ and inverting Equation (14) yields the closed-form expression for the critical activation diameter D_a:

$$D_a = 10^{\chi(\mathrm{SAE},\sigma_g)} \cdot e^{(k_{mie}-1)\ln^2\sigma_g} \cdot \exp\left[\sqrt{2}\sigma_d \cdot \mathrm{erf}^{-1}\left(\frac{2f_{sp} - 2 + MAF}{MAF}\right)\right] \tag{16}$$

This derivation applies across the entire f_{sp} domain of $[1 - MAF, 1]$ and requires only optical inputs (f_{sp}, SAE) alongside aerosol parameters (σ_g, σ_a, MAF). The formula that characterizes the function $\chi(\mathrm{SAE}, \sigma_g)$ would be discussed in Sect 3.1.

By the way, in measurements of size-resolved aerosol activation ratios using a cloud condensation nuclei counter at the ground site, the MAF can sometimes be substantially lower than unity because of the presence of externally mixed hydrophobic aerosol particles (Tao et al., 2018). However, these measurements are typically limited to particle diameters below 400 nm, which may bias the estimated MAF. Comprehensive field measurements of size-resolved aerosol activation over a broader particle size range, particularly under in-cloud conditions, are therefore needed to better constrain the MAF in future studies.

2.3 Regime-Specific Approximate Formulas

Although the exact unified solution of Eq. (16) fully characterizes the entire parameter space, its mathematical complexity hinders direct physical interpretation. To elucidate the underlying linkage

https://doi.org/10.5194/egusphere-2026-5325
Preprint. Discussion started: 9 September 2026

regimes, we derive three asymptotic approximations by examining the limiting behavior of the inverse error function. It should be emphasized that these asymptotic expressions are intended to provide physical insight rather than numerical reconstruction. Constructing a piecewise solution from these local approximations would introduce truncation errors at the regime boundaries.

(1). Linearization (transition regime): Near $f_{sp} \approx 1 - MAF/2$ or $0.3 < f_{sp} < 0.7$, a Taylor expansion simplifies Eq. (16) to a linear form $D_a \approx k \cdot f_{sp} + b$, where:

$$k = 10^{\chi(\mathrm{SAE},\sigma_g)} \cdot e^{(k_{mie}-1)\ln^2\sigma_g} \cdot \frac{\sqrt{2\pi\left(\ln^2\sigma_g + \ln^2\sigma_a\right)}}{MAF} \tag{17}$$

and

$$b = 10^{\chi(\mathrm{SAE},\sigma_g)} \cdot e^{(k_{mie}-1)\ln^2\sigma_g} \cdot \left[1 - \frac{\sqrt{2\pi}\sigma_d}{MAF}\left(1 - \frac{MAF}{2}\right)\right] \tag{18}$$

Asymptotic regimes (Boundary Zones): Near the physical boundaries ($y \to \pm 1$), the linear scheme breaks down. Using the asymptotic approximation $\mathrm{erf}^{-1}(y) \approx \mathrm{sgn}(y)\sqrt{-\ln(1-|y|)}$, we define the boundary behaviors.

(2). For low interstitial scattering fractions ($f_{sp} \to 1 - MAF$):

$$D_a \approx 10^{\chi(\mathrm{SAE},\sigma_g)} \cdot e^{(k_{mie}-1)\ln^2\sigma_g} \cdot \exp\left[-\sqrt{-2{\sigma_d}^2 \cdot \ln\left(\frac{2(f_{sp}-1+MAF)}{MAF}\right)}\right] \tag{19}$$

(3). For high interstitial scattering fractions ($f_{sp} \to 1$):

$$D_a \approx 10^{\chi(\mathrm{SAE},\sigma_g)} \cdot e^{(k_{mie}-1)\ln^2\sigma_g} \cdot \exp\left[\sqrt{-2{\sigma_d}^2 \cdot \ln\left(\frac{2(1-f_{sp})}{MAF}\right)}\right] \tag{20}$$

For the observations shown in (Kuang et al., 2025), most of f_{sp} points located in the range of 0.3 to 0.8 thus corresponds to the linearization regime which explains the general linear relationships between D_a and f_{sp}. In the following, the theoretical formulation was further verified directly using the field measurements and the applications of this optical method in observing cloud critical activation diameter was discussed.

3 Results and discussions

3.1 Theory Verifications using Field measurements

https://doi.org/10.5194/egusphere-2026-5325
Preprint. Discussion started: 9 September 2026

The theoretical relationship between D_a and f_{sp} is further extended and evaluated using simultaneous measurements of D_a and f_{sp}, and aerosol size distributions obtained during the AQ-SOFAR campaign conducted at the Gucheng site on the North China Plain. Details of the measurements of D_a and f_{sp} are provided in Kuang et al. (2025). Briefly, aerosol size distributions and multiwavelength scattering coefficients of both submicron interstitial aerosols and total aerosols were measured using a combination of the advanced aerosol–fog sampling system (Kuang et al., 2024), aerosol sizing instruments, and a three-wavelength integrating nephelometer operating at 450, 525, and 635 nm.

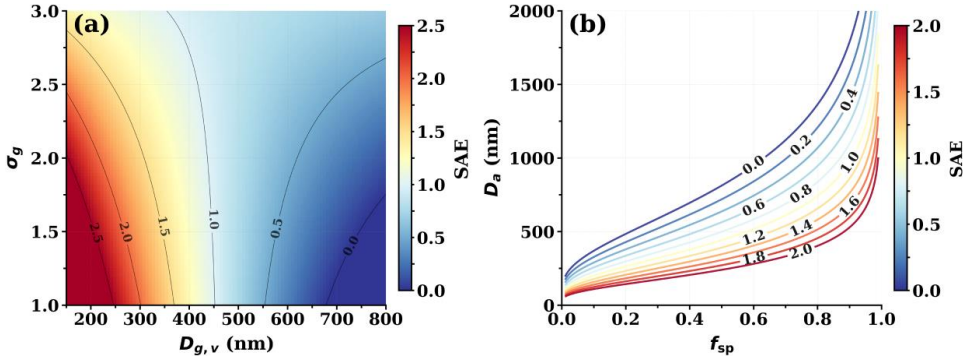

Figure 1. **(a)** Variations of SAE under different $D_{g,v}$ and σ_g, with the square region represents general areas of fitted $D_{g,v}$ and σ_g during fog events of the AQ-SOFAR campaign as shown in Fig.S2; **(b)** The relationships between D_a and f_{sp} under different SAE conditions.

There is no explicit analytical expression for $\chi(\mathrm{SAE}, \sigma_g)$. Therefore, we investigated the dependence of SAE on $D_{g,v}$ and σ_g through Mie scattering calculations of $\sigma_{sp}(450)$ and $\sigma_{sp}(525)$ under different combinations of $D_{g,v}$ and σ_g. The simulated results are presented in Fig. 1a, and details of the calculations are provided in Sect. S2. As shown in Fig. 1a, SAE decreases monotonically with increasing $D_{g,v}$ and decreasing σ_g. The fitted $D_{g,v}$ and σ_g values derived from the AQ-SOFAR campaign are also shown in Fig. S2a. These observations exhibit a positive correlation (R^2=0.23), indicating that variations in $D_{g,v}$ and σ_g are not independent. To account for this covariance, we calculated SAE using the observed pairs of $D_{g,v}$ and σ_g and subsequently parameterized its dependence on both variables with the following empirical relationship:

$$\mathrm{SAE}=a\cdot \log_{10} D_{g,v} + b\cdot \sigma_g + c\cdot \sigma_g \cdot \log_{10} D_{g,v} + d \quad (21)$$

The fitted coefficients are a =-7.11, b=-4.846, c=1.836 and d=19.84. The parameterizations reproduced the simulated SAE well with a coefficient of determination (R^2) of 0.96 (Fig.S2b). Using Eq. (16) we

https://doi.org/10.5194/egusphere-2026-5325
Preprint. Discussion started: 9 September 2026

further examined the relationship between D_a and f_{sp} by fixing MAF=1, σ_a =1.2 and σ_g =1.8, corresponding to the mean values observed during the three consecutive fog events in the AQ-SOFAR campaign. The calculated results are shown in Fig.1b. As shown, the relationship between D_a and f_{sp} is approximately linear over the f_{sp} range of 0.2-0.8. Specifically, for the linear expression $D_a = k \cdot f_{sp} + b$ in the f_{sp} range of 0.2-0.8, the fitted coefficients are k=703.4 and b=103.2 for SAE of 1 and k=519.0 and b=76.1 for SAE of 1.5. To evaluate the applicability of this simplified relationship, the calculated D_a values derived from the mean observed SAE of 1.2 ($D_a = 625.9 \cdot f_{sp} + 84.6$) were compared with the observed D_a values. The comparison (Fig. 2a) yields an R^2 of 0.57, with most data points falling within the ±20% deviation lines, demonstrating that the simplified linear relationship provides a reasonable approximation under typical fog conditions. This agreement also provides a direct field validation of the proposed theoretical framework using independent measurements of aerosol size distributions and aerosol activation characteristics. Nevertheless, the relationship becomes nonlinear, while remaining monotonic, as f_{sp} approaches either 0 or 1.

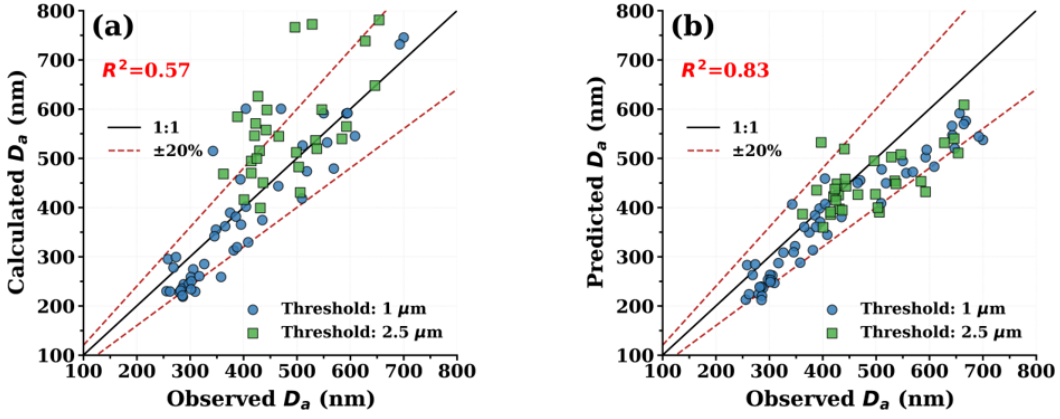

Figure 2. Comparisons between observed D_a and calculated D_a using 1 and 2.5 μm as the threshold of interstitial aerosols with the derived linear formula **(a)** and with the machine learning framework that accounts for SAE variations **(b)**.

As demonstrated by Kuang et al. (2025), a machine-learning framework can account for the dependence on the scattering Ångström exponent (SAE) as well as the nonlinear behavior near regime boundaries. Here, the dataset-generation framework developed by Kuang et al. (2025) was adopted to further extend the analysis. In brief, aerosol particle number size distributions (PNSDs) measured during six field campaigns over the North China Plain (Kuang et al., 2018) were used to represent a wide range of atmospheric aerosol conditions. For each measured PNSD, 100 activation ratio curves were randomly generated using Eq. (2). The scattering coefficients of submicron interstitial aerosols and total aerosols (interstitial + activated) at 450, 525, and 635 nm were then calculated using the same

https://doi.org/10.5194/egusphere-2026-5325
Preprint. Discussion started: 9 September 2026

Mie-theory procedure as described in Kuang et al. (2025), corresponding to the three wavelengths measured by the Aurora 3000 nephelometer during the AQ-SOFAR campaign. A random forest model (Model 1) was subsequently trained using the simulated dataset, with only f_{sp} at 525 nm and the total aerosol scattering coefficients at 450, 525, and 635 nm as input variables and the D_a as the target variable. By incorporating scattering measurements at three wavelengths, the model implicitly accounts for variations in SAE and, therefore, aerosol size distribution. The trained model was then applied to the AQ-SOFAR observations using the measured f_{sp} at 525 nm together with the total aerosol scattering coefficients at the three wavelengths as inputs. As shown in Fig. 2b, the predicted D_a agrees well with the observations compared with the linear formula of SAE=1.2, yielding R^2=0.83, substantially higher than that obtained using the analytical parameterization alone (Fig. 2a). The mean relative deviation is approximately 11%.

However, as indicated by Eq. (16), the relationship between D_a and f_{sp} is influenced not only by SAE but also by MAF, σ_g and σ_a. Therefore, constraining only f_{sp} and SAE is insufficient to uniquely determine D_a, and additional constraints are needed. Physically, MAF, σ_g and σ_a primarily affect the shapes of the dry-state size distributions of the interstitial and activated aerosol populations. As demonstrated by Kuang et al. (2025), these effects can be further constrained through the spectral scattering characteristics of the two aerosol populations. Compared with Model 1, Model 2 (the Model proposed in Kuang et al. (2025)) additionally incorporates dry scattering coefficients of interstitial aerosols, $\sigma_{sp,,inter}(dry,\lambda)$, together with those of total aerosols, $\sigma_{sp,all}(dry,\lambda)$ at 450, 525, and 635 nm. These six scattering parameters simultaneously contain information on f_{sp} (through $\sigma_{sp,inter}(dry,\lambda)$/ $\sigma_{sp,all}(dry,\lambda)$) and the spectral scattering characteristics of both the interstitial and activated aerosol populations (through spectral dependence subtraction of $\sigma_{sp,all}(dry,\lambda)$ - $\sigma_{sp,,inter}(dry,\lambda)$). Together, they provide stronger constraints on the aerosol size distributions governing the D_a and f_{sp} relationship. Consequently, the prediction performance is further improved, with R^2 increasing to 0.88. All predicted values fall within the ±10% deviation lines (Fig. 1d in Kuang et al., 2025), and the mean relative deviation decreases to 8.5%. The relatively modest improvement of Model 2 over Model 1 suggests that accounting for the nonlinearity of the D_a and f_{sp} relationship and its dependence on SAE contributes most to the retrieval accuracy, whereas additional constraints on the size distributions of the interstitial and activated aerosol populations provide a secondary improvement.

https://doi.org/10.5194/egusphere-2026-5325
Preprint. Discussion started: 9 September 2026

In summary, this study establishes the theoretical basis for optically retrieving D_a, whereas the machine-learning framework developed by Kuang et al. (2025) provides a practical implementation by incorporating the nonlinear and multidimensional dependencies revealed by the theory.

3.2 Theoretical detection limit and practical applicability

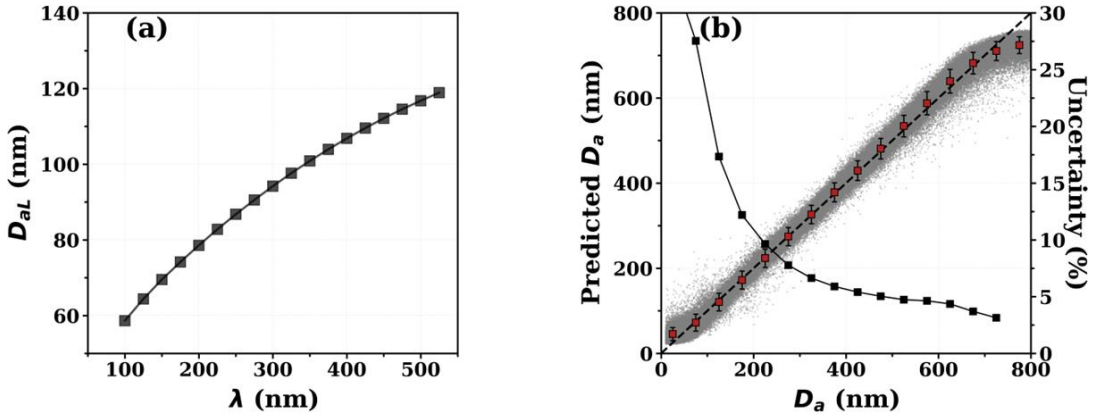

Figure 3. **(a)** Simulated relationships between D_{aL} and λ; **(b)** Comparisons of all prescribed D_a and predicted D_a values represented by scatter points with dry state scattering coefficients of interstitial and total aerosols at wavelengths of 100, 200 and 300 nm as inputs; Scatter points are further binned with interval of 50 nm, averages and standard deviations represented by red squares and their error bars, black squares represent relative uncertainty of the right axis at each bin.

Although the optical retrieval of D_a from aerosol scattering measurements was first proposed and demonstrated by Kuang et al. (2025), its physical limitations and applicable scenarios have not been theoretically discussed. Here, we extend the previous work based on the theoretical framework developed in this study.

The first aspect concerns the lower detection limit of optically retrieving D_a. The physical basis of the proposed method is the monotonic decrease of f_{sp} with decreasing D_a. However, the size-resolved cumulative contribution to aerosol scattering reported by Kuang et al. (2018) indicates that, at a wavelength of 550 nm, particles smaller than approximately 100 nm contribute negligibly to total aerosol scattering. Consequently, f_{sp} approaches zero as D_a decreases to around 100 nm, causing the monotonic relationship between D_a and f_{sp} to break down. Therefore, activation diameters below this threshold cannot be uniquely inferred from scattering measurements. Here, we define the activation diameter corresponding to f_{sp}=0.1% (detectable changes) as the lower detection limit, D_{aL}. As shown in Fig. S3, D_{aL} depends strongly on the measurement wavelength. Shorter wavelengths increase the scattering contribution of smaller particles and therefore reduce the detection limit. The quantitative

https://doi.org/10.5194/egusphere-2026-5325
Preprint. Discussion started: 9 September 2026

relationship between D_{aL} and wavelength is presented in Fig. 3a. The results indicate that D_{aL} decreases to approximately 60 nm when the measurement wavelength reaches 100 nm. Such wavelengths may become feasible for aerosol scattering measurements in the future, given the rapid development of ultraviolet and vacuum-ultraviolet light sources in other technological fields.

As demonstrated in Sect. 3.1, the machine-learning framework incorporates not only f_{sp} but also the spectral scattering characteristics of both the interstitial and total aerosol populations, thereby providing stronger constraints on the underlying aerosol size distributions. Such additional information is expected to further improve the retrieval accuracy near the detection limit. To examine this possibility, Model 2 was retrained using simulated scattering coefficients at 100, 200, and 300 nm instead of 450, 525, and 635 nm. As shown in Fig. 3b, the lower detection limit is further reduced to approximately 50 nm, while the retrieval uncertainty remains below 10% over the D_a range of 200–700 nm.

Assuming κ=0.4 for 50 nm particles, corresponding to highly hygroscopic marine aerosols (Huang et al., 2022) and substantially larger than the values typically observed for continental aerosols with average κ of ultrafine aerosols generally below 0.2 (Peng et al., 2020), the corresponding critical supersaturation is approximately 0.52%. Cloud supersaturation is jointly controlled by cloud dynamics and microphysical processes, and available observations and estimations indicate that it is typically below 1% (Romps, 2025), exceeding 2% only in vigorous deep convective systems (Fan et al., 2025;Fan et al., 2026). The ranges summarized in Chapter 17 of Seinfeld and Pandis (2016) further show that maximum supersaturations below approximately 0.5% encompass fogs, stratus clouds, and a large fraction of marine and continental cumulus clouds. Existing aircraft and ground-based observations likewise rarely report supersaturations exceeding 0.5% (Hammer et al., 2014;Mazoyer et al., 2019;Wainwright et al., 2021;Zíková et al., 2020;Kuang et al., 2024;Politovich and Cooper, 1988;Hudson et al., 2010;Hudson et al., 2015;Gong et al., 2023;Dedrick et al., 2025). Therefore, the proposed optical approach is expected to be applicable to most atmospheric cloud and fog environments.

Another important advantage of the proposed approach that should be emphasized is its high temporal resolution. Clouds are highly heterogeneous and evolve rapidly because of turbulent mixing, entrainment, and variations in cloud dynamics. Consequently, supersaturation and aerosol activation can vary substantially on timescales of only a few seconds, and rapid transitions between supersaturated and subsaturated conditions might frequently occur near cloud boundaries. Capturing these transient processes requires high-time-resolution observations of D_a. In contrast to retrievals

https://doi.org/10.5194/egusphere-2026-5325
Preprint. Discussion started: 9 September 2026

based on aerosol size distribution measurements, which generally require tens of seconds to several minutes, most aerosol scattering instruments provide reliable measurements with time resolutions of second level (Moise et al., 2015). As suggested by Kuang et al. (2025), this high-time-resolution capability makes the proposed method particularly suitable for high-resolution cloud observations and may ultimately enable vertical profiling of cloud supersaturation and aerosol activation when combined with airborne or uncrewed aerial platforms.

4. Conclusions

Aerosol activation is the fundamental microphysical process governing cloud droplet formation and forms the basis of the Twomey effect, thereby playing a central role in aerosol–cloud interactions. However, direct in-situ observations of aerosol activation in clouds remain extremely limited because of the lack of efficient observational techniques. In this study, we have established the theoretical framework for optically retrieving the aerosol critical activation diameter by bridging aerosol activation theory and Mie scattering theory. The derived formulation explains the nearly linear relationship between the critical activation diameter and the submicron scattering fraction of interstitial aerosols reported by Kuang et al. (2025), thereby providing the physical foundation for optical observations of aerosol activation in clouds.

Based on the proposed theory, the applicability and detection limit of the optical retrieval are further quantified. The results demonstrate that the proposed approach is capable of retrieving the critical activation diameter over the supersaturation range encountered in most atmospheric clouds. Although explicit analytical expressions describing the relationship between the critical activation diameter and the interstitial aerosol scattering fraction were derived, the machine-learning framework developed by Kuang et al. (2025) remains the preferred approach for practical applications because it effectively incorporates the nonlinear and multidimensional dependencies identified by the theory.

It should be noted that the proposed theory fundamentally determines the diameter above which particles grow under supersaturated conditions, whereas the diameter used to distinguish cloud droplets from aerosols depends on the inlet cut size and should not be regarded as an intrinsic activation threshold. As shown in Fig. S5 of Kuang et al. (2024), the wet diameter corresponding to cloud droplet activation varies strongly with supersaturation, exceeding 2.5 μmfor supersaturations below approximately 0.06% but decreasing to below 1 μmwhen supersaturation exceeds approximately 0.15%. Consequently, careful selection of the impactor cut size is essential for interpreting optical observations of aerosol activation.

https://doi.org/10.5194/egusphere-2026-5325
Preprint. Discussion started: 9 September 2026

This characteristic also suggests a broader application of the proposed theory. When a PM_1 inlet is employed, for example, particles that grow beyond 1 μm under low-supersaturation conditions (<0.15%) should be interpreted as hygroscopic aerosols rather than activated cloud droplets. Therefore, measurements with multiple impactor inlets combined with multiwavelength scattering observations could simultaneously constrain aerosol hygroscopic growth and activation with high temporal resolution. Such observations would provide a new capability for investigating aerosol–water interactions across the transition from subsaturated to supersaturated conditions and offer valuable insights into cloud microphysical processes.

Competing interests. The contact author has declared that none of the authors has any competing interests.

Availability Statement. All data presented are shown in Figures of this manuscript and more specific data will be made available on request.

Acknowledgments. This work is supported by National Natural Science Foundation of China (42622511).

Author contribution. YK conceived the theory and wrote the manuscript. QL helped plotted the figures.

https://doi.org/10.5194/egusphere-2026-5325
Preprint. Discussion started: 9 September 2026

References:

Abdul-Razzak, H., Ghan, S. J., and Rivera-Carpio, C.: A parameterization of aerosol activation: 1. Single aerosol type, Journal of Geophysical Research: Atmospheres, 103, 6123-6131, https://doi.org/10.1029/97JD03735, 1998.

Abdul-Razzak, H., and Ghan, S. J.: A parameterization of aerosol activation: 2. Multiple aerosol types, Journal of Geophysical Research: Atmospheres, 105, 6837-6844, https://doi.org/10.1029/1999JD901161, 2000.

Abdul-Razzak, H., and Ghan, S. J.: A parameterization of aerosol activation 3. Sectional representation, Journal of Geophysical Research: Atmospheres, 107, AAC 1-1-AAC 1-6, https://doi.org/10.1029/2001JD000483, 2002.

Anderson, J. C., Beeler, P., Ovchinnikov, M., Cantrell, W., Krueger, S., Shaw, R. A., Yang, F., and Fierce, L.: Enhancements in Cloud Condensation Nuclei Activity From Turbulent Fluctuations in Supersaturation, Geophysical Research Letters, 50, e2022GL102635, https://doi.org/10.1029/2022GL102635, 2023.

Bian, Y. X., Zhao, C. S., Ma, N., Chen, J., and Xu, W. Y.: A study of aerosol liquid water content based on hygroscopicity measurements at high relative humidity in the North China Plain, Atmos. Chem. Phys., 14, 6417-6426, 10.5194/acp-14-6417-2014, 2014.

Boulter, J. E., Cziczo, D. J., Middlebrook, A. M., Thomson, D. S., and Murphy, D. M.: Design and Performance of a Pumped Counterflow Virtual Impactor, Aerosol Science and Technology, 40, 969-976, 10.1080/02786820600840984, 2006.

Cai, J., Chu, B., Yao, L., Yan, C., Heikkinen, L. M., Zheng, F., Li, C., Fan, X., Zhang, S., Yang, D., Wang, Y., Kokkonen, T. V., Chan, T., Zhou, Y., Dada, L., Liu, Y., He, H., Paasonen, P., Kujansuu, J. T., Petäjä, T., Mohr, C., Kangasluoma, J., Bianchi, F., Sun, Y., Croteau, P. L., Worsnop, D. R., Kerminen, V.-M., Du, W., Kulmala, M., and Daellenbach, K. R.: Size-segregated particle number and mass concentrations from different emission sources in urban Beijing, Atmospheric Chemistry and Physics, 20, 12721-12740, 10.5194/acp-20-12721-2020, 2020.

Dedrick, J. L., Pelayo, C. N., Russell, L. M., Lubin, D., Mülmenstädt, J., and Miller, M.: Competition response of cloud supersaturation explains diminished Twomey effect for smoky aerosol in the tropical Atlantic, Proceedings of the National Academy of Sciences, 122, e2412247122, doi:10.1073/pnas.2412247122, 2025.

Ditas, F., Shaw, R. A., Siebert, H., Simmel, M., Wehner, B., and Wiedensohler, A.: Aerosols-cloud microphysics-thermodynamics-turbulence: evaluating supersaturation in a marine stratocumulus cloud, Atmos. Chem. Phys., 12, 2459-2468, 10.5194/acp-12-2459-2012, 2012.

Espinosa, W. R., Remer, L. A., Dubovik, O., Ziemba, L., Beyersdorf, A., Orozco, D., Schuster, G., Lapyonok, T., Fuertes, D., and Martins, J. V.: Retrievals of aerosol optical and microphysical properties from Imaging Polar Nephelometer scattering measurements, Atmos. Meas. Tech., 10, 811-824, 10.5194/amt-10-811-2017, 2017.

Fan, C., Li, S., Zang, L., Pan, Z., Mao, F., Liu, F., Gong, W., and Rosenfeld, D.: Idealized simulations reveal the potential for widespread high supersaturation in marine tropical deep convection, Atmospheric Research, 109091, https://doi.org/10.1016/j.atmosres.2026.109091, 2026.

Fan, J., Wang, Y., Rosenfeld, D., and Liu, X.: Review of Aerosol–Cloud Interactions: Mechanisms, Significance, and Challenges, Journal of the Atmospheric Sciences, 73, 4221-4252, https://doi.org/10.1175/JAS-D-16-0037.1, 2016.

Fan, J., Zhang, Y., Li, Z., Yan, H., Prabhakaran, T., Rosenfeld, D., and Khain, A.: Unveiling Aerosol Impacts on Deep Convective Clouds: Scientific Concept, Modeling, Observational Analysis, and Future Direction, Journal of Geophysical Research: Atmospheres, 130, e2024JD041931, https://doi.org/10.1029/2024JD041931, 2025.

https://doi.org/10.5194/egusphere-2026-5325
Preprint. Discussion started: 9 September 2026

Gao, R. S., Perring, A. E., Thornberry, T. D., Rollins, A. W., Schwarz, J. P., Ciciora, S. J., and Fahey, D. W.: A High-Sensitivity Low-Cost Optical Particle Counter Design, Aerosol Science and Technology, 47, 137-145, 10.1080/02786826.2012.733039, 2013.
Gong, X., Wang, Y., Xie, H., Zhang, J., Lu, Z., Wood, R., Stratmann, F., Wex, H., Liu, X., and Wang, J.: Maximum Supersaturation in the Marine Boundary Layer Clouds Over the North Atlantic, AGU Advances, 4, e2022AV000855, https://doi.org/10.1029/2022AV000855, 2023.
Hammer, E., Gysel, M., Roberts, G. C., Elias, T., Hofer, J., Hoyle, C. R., Bukowiecki, N., Dupont, J. C., Burnet, F., Baltensperger, U., and Weingartner, E.: Size-dependent particle activation properties in fog during the ParisFog 2012/13 field campaign, Atmos. Chem. Phys., 14, 10517-10533, 10.5194/acp-14-10517-2014, 2014.
Henning, S., Bojinski, S., Diehl, K., Ghan, S., Nyeki, S., Weingartner, E., Wurzler, S., and Baltensperger, U.: Aerosol partitioning in natural mixed-phase clouds, Geophysical Research Letters, 31, https://doi.org/10.1029/2003GL019025, 2004.
Hou, M., Liu, L., Yuan, F., Zhai, M., Xu, H., Zhao, G., and Kuang, Y.: Distinct but Likely Interdependent Roles of Secondary Organic and Inorganic Aerosol Formation in Aerosol Scattering, in: Remote Sensing, 11, 1713, 2026.
Huang, S., Wu, Z., Wang, Y., Poulain, L., Höpner, F., Merkel, M., Herrmann, H., and Wiedensohler, A.: Aerosol Hygroscopicity and its Link to Chemical Composition in a Remote Marine Environment Based on Three Transatlantic Measurements, Environmental science & technology, 10.1021/acs.est.2c00785, 2022.
Hudson, J. G., Noble, S., and Jha, V.: Stratus cloud supersaturations, Geophysical Research Letters, 37, https://doi.org/10.1029/2010GL045197, 2010.
Hudson, J. G., Noble, S., and Tabor, S.: Cloud supersaturations from CCN spectra Hoppel minima, Journal of Geophysical Research: Atmospheres, 120, 3436-3452, https://doi.org/10.1002/2014JD022669, 2015.
Kreidenweis, S. M., Petters, M., and Lohmann, U.: 100 Years of Progress in Cloud Physics, Aerosols, and Aerosol Chemistry Research, Meteorological Monographs, 59, 11.11-11.72, 10.1175/amsmonographs-d-18-0024.1, 2018.
Kuang, Y., Zhao, C. S., Zhao, G., Tao, J. C., Xu, W., Ma, N., and Bian, Y. X.: A novel method for calculating ambient aerosol liquid water content based on measurements of a humidified nephelometer system, Atmospheric Measurement Techniques, 11, 2967-2982, 10.5194/amt-11-2967-2018, 2018.
Kuang, Y., He, Y., Xu, W., Zhao, P., Cheng, Y., Zhao, G., Tao, J., Ma, N., Su, H., Zhang, Y., Sun, J., Cheng, P., Yang, W., Zhang, S., Wu, C., Sun, Y., and Zhao, C.: Distinct diurnal variation in organic aerosol hygroscopicity and its relationship with oxygenated organic aerosol, Atmos. Chem. Phys., 20, 865-880, 10.5194/acp-20-865-2020, 2020.
Kuang, Y., Xu, W., Tao, J., Luo, B., Liu, L., Xu, H., Xu, W., Xue, B., Zhai, M., Liu, P., and Sun, Y.: Divergent Impacts of Biomass Burning and Fossil Fuel Combustion Aerosols on Fog-Cloud Microphysics and Chemistry: Novel Insights From Advanced Aerosol-Fog Sampling, Geophysical Research Letters, 51, e2023GL107147, https://doi.org/10.1029/2023GL107147, 2024.
Kuang, Y., Tao, J., Xu, H., Liu, L., Liu, P., Xu, W., Xu, W., Sun, Y., and Zhao, C.: Theoretical framework for measuring cloud effective supersaturation fluctuations with an advanced optical system, Atmos. Chem. Phys., 25, 1163-1174, 10.5194/acp-25-1163-2025, 2025.
Mazoyer, M., Burnet, F., Denjean, C., Roberts, G. C., Haeffelin, M., Dupont, J. C., and Elias, T.: Experimental study of the aerosol impact on fog microphysics, Atmos. Chem. Phys., 19, 4323-4344, 10.5194/acp-19-4323-2019, 2019.
Moise, T., Flores, J. M., and Rudich, Y.: Optical Properties of Secondary Organic Aerosols and Their Changes by Chemical Processes, Chemical Reviews, 115, 4400-4439, 10.1021/cr5005259, 2015.
Motos, G., Schmale, J., Corbin, J. C., Modini, R. L., Karlen, N., Bertò, M., Baltensperger, U., and Gysel-Beer, M.: Cloud droplet activation properties and scavenged fraction of black carbon in liquid-

https://doi.org/10.5194/egusphere-2026-5325
Preprint. Discussion started: 9 September 2026

phase clouds at the high-alpine research station Jungfraujoch (3580 m a.s.l.), Atmos. Chem. Phys., 19, 3833-3855, 10.5194/acp-19-3833-2019, 2019a.
Motos, G., Schmale, J., Corbin, J. C., Zanatta, M., Baltensperger, U., and Gysel-Beer, M.: Droplet activation behaviour of atmospheric black carbon particles in fog as a function of their size and mixing state, Atmos. Chem. Phys., 19, 2183-2207, 10.5194/acp-19-2183-2019, 2019b.
Noone, K. J., Ogren, J. A., Heintzenberg, J., Charlson, R. J., and Covert, D. S.: Design and Calibration of a Counterflow Virtual Impactor for Sampling of Atmospheric Fog and Cloud Droplets, Aerosol Science and Technology, 8, 235-244, 10.1080/02786828808959186, 1988.
Peng, C., Wang, Y., Wu, Z., Chen, L., Huang, R.-J., Wang, W., Wang, Z., Hu, W., Zhang, G., Ge, M., Hu, M., Wang, X., and Tang, M.: Tropospheric aerosol hygroscopicity in China, Atmospheric Chemistry and Physics, 20, 13877-13903, 10.5194/acp-20-13877-2020, 2020.
Politovich, M. K., and Cooper, W. A.: Variability of the Supersaturation in Cumulus Clouds, Journal of Atmospheric Sciences, 45, 1651-1664, https://doi.org/10.1175/1520-0469(1988)045<1651:VOTSIC>2.0.CO;2, 1988.
Romps, D. M.: A Method for Calculating Reliable Supersaturation Reveals Low Values in Tropical Rainy-Season Clouds, Journal of the Atmospheric Sciences, 82, 1517-1527, https://doi.org/10.1175/JAS-D-24-0265.1, 2025.
Rose, D., Gunthe, S. S., Mikhailov, E., Frank, G. P., Dusek, U., Andreae, M. O., and Pöschl, U.: Calibration and measurement uncertainties of a continuous-flow cloud condensation nuclei counter (DMT-CCNC): CCN activation of ammonium sulfate and sodium chloride aerosol particles in theory and experiment, Atmos. Chem. Phys., 8, 1153-1179, 10.5194/acp-8-1153-2008, 2008.
Seinfeld, J., and Pandis, S.: Atmospheric Chemistry and Physics: From Air Pollution to Climate Change, Third Edition, 2016.
Shawon, A. S. M., Prabhakaran, P., Kinney, G., Shaw, R. A., and Cantrell, W.: Dependence of Aerosol-Droplet Partitioning on Turbulence in a Laboratory Cloud, Journal of Geophysical Research: Atmospheres, 126, e2020JD033799, https://doi.org/10.1029/2020JD033799, 2021.
Tao, J., Zhao, C., Ma, N., and Kuang, Y.: Consistency and applicability of parameterization schemes for the size-resolved aerosol activation ratio based on field measurements in the North China Plain, Atmospheric Environment, 173, 316-324, https://doi.org/10.1016/j.atmosenv.2017.11.021, 2018.
Twomey, S.: The nuclei of natural cloud formation part II: The supersaturation in natural clouds and the variation of cloud droplet concentration, Geofisica pura e applicata, 43, 243-249, 10.1007/BF01993560, 1959.
Wainwright, C., Chang, R. Y.-W., and Richter, D.: Aerosol Activation in Radiation Fog at the Atmospheric Radiation Program Southern Great Plains Site, Journal of Geophysical Research: Atmospheres, 126, e2021JD035358, https://doi.org/10.1029/2021JD035358, 2021.
Zíková, N., Pokorná, P., Makeš, O., Sedlák, P., Pešice, P., and Ždímal, V.: Activation of atmospheric aerosols in fog and low clouds, Atmospheric Environment, 230, 117490, https://doi.org/10.1016/j.atmosenv.2020.117490, 2020.